CrossMark

RESEARCH ARTICLE

Effect of electrolysis parameters of Ni–Mo alloy on the electrocatalytic activity for hydrogen evaluation and their stability in alkali medium

Mert Manazoğlu[1] · Gökçe Hapçı[1] · Gökhan Orhan[1]

Abstract In this paper, NiMo coatings were electrochemically deposited on a copper electrode (Cu/NiMo) and on an electrodeposited nickel onto copper plate (Cu/Ni/NiMo) in citrate solutions. Effects of electrolyte composition, pH value, and temperature on hydrogen-evolution reaction (HER) as well as the electrochemical stability in alkaline solution were investigated, and the electrochemical activation energy was determined for the NiMo alloys. This was evaluated by the determination of kinetic and mechanism of HER in alkali medium by the polarization measurements, cyclic voltammetry, and electrochemical impedance spectroscopy techniques. The morphology and chemical composition of the electrodeposited Ni–Mo were investigated using SEM and EDS analyses. The results showed that the corresponding HER overpotential of the Ni–Mo film depends on alloy composition and surface morphology. As the wt% of Mo content in the alloy is increased, the onset potential of electrode for HER shifted in the positive direction favoring hydrogen generation with lower overpotential. The overall experimental data indicated that the porous Ni–Mo coating on electrodeposited nickel plate was obtained when the molybdenum content was ca. 41 wt%. This electrodes exhibited high catalytic activity in the HER ($\eta_{100} = -48$ mV at 100 mA cm^{-2} and 80 °C), and their stability was tested by polarization measurements after different anodic and cathodic treatments in 1 M NaOH solution. Moreover, the corrosion behaviors of Ni and Cu/Ni/NiMo electrodes at open-circuit potential were also investigated, and their corrosion resistances were compared.

Graphical abstract
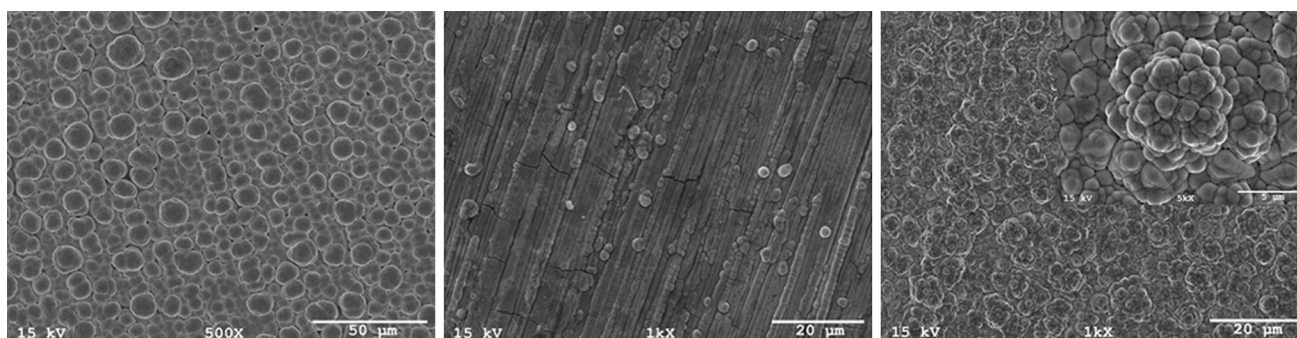
SEM images of NiMo alloys with different wt. % Mo

✉ Gökhan Orhan
   gorhan@istanbul.edu.tr

1   Metallurgical and Materials Engineering Department, Faculty
   of Engineering, Istanbul University, 34320 Istanbul, Turkey

✑ Springer

1 Introduction

Hydrogen is considered as an ideal energy carrier that can be an alternative to fossil fuels. It is a clean and fully recyclable substance with practically unlimited supply and fulfills all the criteria considered for an alternative energy source [1, 2].

Alkaline water electrolysis is an ideal technique to produce high-purity hydrogen. However, except the use of noble metals as the cathode material in water electrolysis, the high overpotential of the hydrogen-evolution reaction (HER) (i.e., high energy consumption) is the most significant disadvantage which restrains its large-scale applications [3–5]. The key parameters for selecting a material for water electrolysis are its good electrical conductivity, low overvoltage electrochemical stability, low cost, and ease of use. The performance of electrocatalysts certainly depends on the chemical composition of the catalyst and its surface area. Hence, the electrode activity of the electrode materials can be improved by modifying the intrinsic activity and/or by increasing the ratio between the real and the geometric surface areas [4–6]. For the HER in the alkaline media, Raney Ni and Ni alloys are the most used catalysts [7–9], among which NiMo is reported to be the best [5, 9–11]. According to the Engel–Brewer valence bond theory, whenever transition metals with empty or less-filled d orbitals (e.g., Mo) are alloyed with those with more-filled d orbitals (e.g., Ni), a synergistic effect in the hydrogen-evolving activity of these materials is expected [12].

The electrodeposition process for production of the Ni–Mo alloys has also some apparent advantages, i.e., nanocrystalline/amorphous materials can be obtained, and there is a possibility to control the chemical composition, grain size, and surface properties of the alloys [13, 14]. In spite of these advantages of the electrochemical method, elemental molybdenum cannot be deposited electrochemically from aqueous media, but these metals can be codeposited as alloys with iron group transition metals such as iron, cobalt, and nickel [15–19]. Alloy electrodeposition of this type is categorized by Brenner as induced codeposition [19].

Han [20] reported that pulse-plated amorphous NiMo alloy coated with 31.04 wt% molybdenum shows high catalytic activity of hydrogen evolution (80 °C, $\eta_{200} = -62$ mV) in 33 wt% NaOH solution. Krstajic [21] found that the NiMo alloy coating, which was electrodeposited from the pyrophosphate-sodium bicarbonate bath on to Ni mesh, possesses high catalytic activity for hydrogen evolution in 33 wt% NaOH solutions at 85 °C. Aaboubi [22] reported that electrochemically produced NiMo alloy under magnetic field showed increased activity of HER. Krstajic studied with non-noble metal composite cathodes for hydrogen evolution where Ni–MoO$_x$ coatings electrodeposited from Watt's type bath containing MoO$_3$ powder particles [23] and Ni–MoO$_2$ coatings electrodeposited from nickel chloride–ammonium bath containing MoO$_2$ powder particles [24]. Both these electrodes were investigated in 32 wt% NaOH at 90 °C for HER, and the results were compared with the commercial De Nora's coating. Xia [25] reported the comparison of Ni–Mo and Ni–Mo–Cu alloy coating electrode prepared on copper substrate by constant-current electrodeposition. Chialvo [26] investigated the dependence of the electrocatalytic activity of the bulk Ni–Mo alloys for the HER as a function of their composition (at varying atomic percentages of molybdenum from 0 to 25 at.%). Hu and Weng [12] found that electroplated Ni–Mo deposits from a bath with a pH of 8, a Ni/Mo ratio of 3.3, and a sodium citrate concentration of 40 g L^{-1} show the highest apparent current density of hydrogen evolution in 1 M NaOH solution. Beltowska-Lehman [27] characterized the composition of Ni–Mo using citrate–ammonia electrolyte with varying pH values.

In this paper, nickel–molybdenum alloy coatings were obtained by electrochemical method. The impacts of different Ni/Mo ratios and electrolyte pH values on the HER activity of Ni–Mo coatings on two substrates: first on copper and second on electrodeposited nickel on copper, were investigated. The aim of the present work is to study the electrocatalytic performance of the developed Ni–Mo coatings for HER, considering the two terms; namely, intrinsic activity and surface properties of the electrode. The mechanisms and kinetics of HER on these electrodes have also been determined. In addition, the HER stability and corrosion behavior of Cu/Ni/NiMo electrode in an alkaline electrolyte were examined with various methods.

2 Materials and methods

2.1 The preparation of Ni and Ni–Mo electrodes

In this study, two types of substrates were used for NiMo electrodeposition. First one is 4 cm^2 (2 × 2) of copper plates, and the second one is 4 cm^2 (2 × 2) of electrolytic nickel which was electrodeposited onto copper plates. The nickel electrodeposits were obtained from conventional Watt's-type baths including 0.95 M NiSO$_4$.6H$_2$O, 0.17 M NiCl$_2$.6H$_2$O and 0.65 M H$_3$BO$_3$. Applied current density was 20 mA cm^{-2}, and the temperature was 50 ± 0.5 °C. Before the electrodeposition experiments, copper substrates were carefully prepared by mechanical wet polishing using 1200 grinding paper. Afterward, samples were

vibrated in an ultrasonic bath with acetone, ethanol, and pure water for each 10 min. Finally, before the electrode-position, copper plates were immersed into 20 % HCl solution for about 1 min, and finally rinsed with pure water again and immersed in the bath solution. The same surface treatments were carried out for nickel substrates; however, mechanical polishing was not performed. Ni–Mo alloys were obtained in a conventional three-electrode cell. The anode was large-area platinized titanium mesh, and the reference electrode was Ag/AgCl (3 M KCl) that was connected to the cathode by a Luggin capillary positioned 0.2 cm from the cathode surface. The distance between cathode and anode was fixed at 3 cm. The plating baths used for the Ni–Mo alloy electrodeposition consisted of $NiSO_4.6H_2O$ and $Na_2MoO_4.2H_2O$ compounds as Ni^{2+} and Mo^{6+} sources, respectively, and 0.3 M $Na_2C_6H_5O_7.2H_2O$ was also added to all plating baths as a complexing agent. 3/2, 1/1, 2/3 and 1/12 molar ratios of Ni/Mo in the plating bath was investigated while the total concentration of nickel and molybdenum ions in the electrolyte was kept constant as 0.5 M. Two different constant pH values of the electrolyte were used: 9.5 and 10.5. This was adjusted by 25 % NH_3 solution. The electrodeposition experiments were performed in galvanostatic regime at 200 mA cm^{-2} for 15 min (180 C cm^{-2}) at 30 ± 0.5 °C. The electrolyte was stirred with magnetic stirrer at 120 rpm for all experiments. After electrolysis, the samples were rinsed with distilled water and prepared for the electrochemical measurements.

2.2 The characterization of Ni–Mo electrode

The surface morphology as well as the composition of the coatings was characterized with scanning electron microscopy (SEM, Jeol JSM 5600), equipped with EDS (iXRF 500).

Electrochemical characterizations of NiMo electrode for hydrogen evolution in alkali solution were carried out by cathodic polarization, cyclic voltammetry, and electro-chemical impedance spectroscopy (EIS) techniques, respectively. The electrochemical measurements were carried out in a conventional electrochemical cell, using 1 M NaOH solution as electrolyte. NiMo alloy electrode 1 cm^2 was used as work electrode, the counter electrode was a large Pt foil, while Ag/AgCl (3 M KCl) electrode was used as a reference electrode with a lugging capillary being close to the working electrode. All potential data given in this study were referred to this reference electrode.

The polarization curves were performed in the potential range from −1.50 V up to the equilibrium potential at a scan rate of 0.5 mV s^{-1} in 1 M NaOH solution at the different temperatures, and the corresponding electrochemical parameters were derived from the recorded curves. Before recording polarization diagrams, electrodes were exposed to hydrogen evolution in the same solution at current density of −100 mA cm^{-2} for the 10 or 60 min. In the case of the anodic or cathodic treatment (oxygen or hydrogen evolution on the electrode surface), polarization diagrams were recorded immediately after these treatments. The polarization diagrams were recorded on a Gamry Potentiostat Reference 600 with automatic IR drop compensation (current interrupt technique), using Corrosion Techniques Software DC 105.

The EIS measurements were performed with the same potentiostat using EIS 300 software. Before the EIS experiments, the electrodes were exposed to HER at −100 mA cm^{-2} for 30 min. Nyquist and Bode diagrams were recorded at −1.20, −1.25, and −1.30 V potentials. The frequency range was 0.1 Hz–100 kHz and the amplitude was 5 mV. In addition, in order to investigate the corrosion behavior Ni and NiMo electrodes, EIS tests were performed at open-circuit potential in 1 M NaOH medium at 25 °C. The acquired data were curve fitted and analyzed using EIS 300 software.

Electrodes were exposed to cyclic procedure up to potential of the oxygen evolution in order to investigate the influence of anodic polarization on the HER activity. The CV's were recorded in the 1 M NaOH solution at 25 °C with a sweep rate of 10 mV s^{-1}. CV experiments were performed for ten cycles between −1.30 and +0.65 V on 1 cm^2 of NiMo electrodes with the same potentiostat using DC 105 software.

In order to determine the kinetic parameters of the HER, steady-state polarization curves were used. For the linear part of the steady-state polarization curves, the kinetic equation can be written as

$$\log(j) = \log(j_0) + \eta/b \qquad (1)$$

where, j is the measured current density (mA cm^{-2}), j_0 is the exchange current density (mA cm^{-2}) (i.e., the equal, partial anodic and cathodic current densities at the equilibrium potentials), η (mV) is the applied overpotential and b is the Tafel slope (mV dec^{-1}). The other parameters of interest is β, the symmetry factor, and/or α, the electron-transfer coefficient which can be calculated from the Tafel slope. For any Tafel polarization curves in the case of alkaline solutions, the hydrogen-evolution overpotentials are calculated using $\eta = E - E_{eq} - R_sI$ [24] where E is the applied potential value, E_{eq} is the equilibrium potential of the HER in corresponding solutions, and R_sI term is the ohmic drop which was already compensated by potentiostat [5, 22].
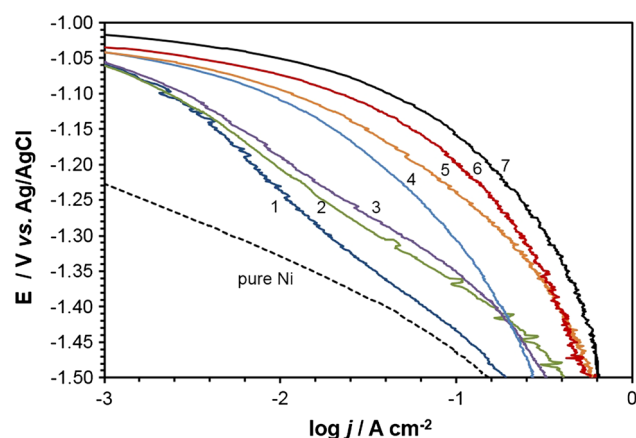
Fig. 1 The polarization curves of different Ni–Mo alloys and a pure Ni film recorded in 1 M NaOH at 30 °C
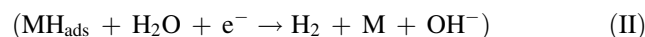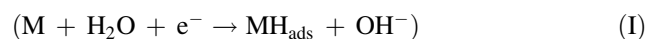
3 Results and discussion

3.1 Effect of electrodeposition conditions of Ni–Mo alloy on HER

Figure 1 shows the cathodic polarization curves that were recorded in 1 M NaOH solution at 30 °C for different contents of Ni/Mo concentrations, pH value, and substrate material. A curve performed on nickel coated copper electrode was also included to compare the results. The experimental conditions are summarized in Table 1. In addition, wt% Mo in alloy and electrode potential (E) at -100 mA cm^{-2} and equilibrium potential (E_{eq}) during polarization test are given in Table 1. The HER kinetic parameters; the Tafel slope (b), the exchange current density (j_0), were determined for each electrode from the linear part of polarization plots (Fig. 1) (for low (1–10 mA) and high (10–100 mA) current density areas). j_0 values were derived by extrapolation of Tafel plots to zero overvoltage. From the Tafel slopes in Fig. 1, the electron transfer coefficient was estimated through $\alpha = (-2.3RT)/(bnF)$, where R is the gas constant (8.314 J mol^{-1} K^{-1}), n is the number of electrons

transferred in the reaction, T is temperature (K), and F is Faraday's constant (96.485 C mol^{-1}). Also, the overpotentials at a fixed current density of -100 mA cm^{-2} (η_{100}) and the current densities at -100 mV overpotential (j_{100}) were determined from the Fig. 1 and are given in Table 2.

In general, in the alkaline media, hydrogen evolution reaction proceeds via three consecutive reactions: Volmer (I), Heyrovsky (II), and Tafel (III)

$$(M + H_2O + e^- \rightarrow MH_{ads} + OH^-) \qquad (I)$$

$$(MH_{ads} + H_2O + e^- \rightarrow H_2 + M + OH^-) \qquad (II)$$

$$(2MH_{ads} \rightarrow 2M + H_2) \qquad (III)$$

HER starts with the proton discharge electrosorption (I), and follows either or both, electrodesorption step (II), and/or H recombination step (III). When the Tafel slopes at 25 °C are 120 mV, then Volmer reaction is known to be the rate-determining step (rds). If this value is 40 mV, Heyrovsky or 30 mV Tafel is considered as the rds [28–30].

It has been accepted in the literature that the value of the charge-transfer coefficient, α, depends on the rds for multistep reactions [7, 30, 31]. It is important to note that for the Volmer step as the rds, the symmetry factor, β, is equal to the transfer coefficient, α, while for the Heyrovsky step, the transfer coefficient is $\alpha = 1 + \beta$ [32–34].

It can be seen from Fig. 1 and Table 2 that all Ni–Mo alloys show better HER activity than pure nickel. However, the minimum HER potentials between curves 1–4 (Fig. 1) at current density of -100 mA cm^{-2} is -1.307 V where curve 4 corresponds to about 28 wt% Mo (Table 1). Jaksic [35] has discussed the effect of alloying with transition metals on both hydrogen evolution activity and catalyst stability on the basis of the Engel–Brewer valence bond theory. According to this theory, the electrocatalytic activity of Ni–Mo deposits is qualitatively proportional to the Mo content [12]. It is important to note that except 1/12 of Ni/Mo ratio (curve 4–7), all other Ni–Mo alloys and pure Ni films show nearly the same Tafel slopes. Current–potential curves of 1–3 NiMo electrodes and Ni electrode

Table 1 Electrolyte compositions of Ni and Ni–Mo alloy samples and corresponding potentials for hydrogen evolution at -100 mA cm^{-2}

| Substrata/sample no	Ni/Mo ratio	pH ± 0.05	Exposure time of HER (min)	wt% Mo in alloy	$-E$ (V)	$-E_{eq}$ (V)
Cu/1	3/2	10.5	10	9.7 ± 1.5	1.434	1.018
Cu/2	1/1	10.5	10	11.9 ± 1.9	1.367	1.011
Cu/3	2/3	10.5	10	13.8 ± 1.9	1.352	1.016
Cu/4	1/12	10.5	10	28.3 ± 2.1	1.307	1.017
Cu/5	1/12	9.5	10	40.1 ± 3.2	1.240	1.023
Cu/6	1/12	9.5	60	40.1 ± 3.2	1.200	1.021
Cu/Ni/7	1/12	9.5	60	41.1 ± 3.3	1.154	1.007
Cu/Ni	–	5.2	10	–	1.465	0.999

Table 2 HER kinetic parameters obtained by analysis of curves presented in Fig. 1

Sample no	$-b_1$ (mV dec^{-1})	$j_{0,1}$ (mA cm^{-2})	α_1	$-b_2$ (mV dec^{-1})	$j_{0,2}$ (mA cm^{-2})	α_2	η_{100} (mV)	j_{100} (mA)
1	185	0.56	0.32	187	0.61	0.32	416	3.1
2	152	0.55	0.39	154	0.57	0.39	356	2.8
3	141	0.60	0.41	144	0.60	0.41	336	3.7
4	71	0.56	0.83	196	4.2	0.30	290	11.8
5	56	0.59	1.05	152	4.3	0.39	217	19.5
6	40	0.59	1.48	143	6.5	0.41	179	34.8
7	36	0.66	1.64	145	11.1	0.41	147	47.1
Ni	118	0.21	0.50	121	0.28	0.49	466	0.12

1 and 2: low and high current density areas, respectively

(Fig. 1) show a typical Tafel behavior indicating that the HER is kinetically controlled. It can be said that based on the Tafel slopes and charge-transfer coefficients of samples 1–3, the Volmer step must control the HER on this electrodes, i.e., the adsorption of H$^+$ onto the active sites of surface is a slow step than the order in HER. On the other hand, curves 4–7 show two different Tafel slopes, which implies that the increase in the overpotential in intermedia increased the surface coverage of the adsorbed hydrogen (θ_H) from 0 to 1 [28]. This point will be discussed in more detail later in the text.

The composition and structure of Ni–Mo electrodeposits should also depend on pH. For Ni–Mo-induced codeposition, a basic plating bath's pH has been proposed to be an important variable influencing the quality and composition of the deposits because of the presence of free NH$_3$. The curve 5 shows a set of Tafel curves recorded at pH value of 9.5, while curve 4 is obtained for pH value of 10.5. According to EDS results of sample 5, Mo amount in the alloy was increased up to 40.1 wt%, when the electrolyte pH was 9.5. However, HER voltage of this alloy at a current density of 100 mA cm^{-2} decreased to ca. 67 mV with decreased pH (Table 1). For an induced codeposition mechanism, Ni^{2+} can be reduced on the cathode surface via the (NiCit)$^-$ and [Ni(NH$_3$)$_n$]$^{2+}$ (n = 2–6) complexes, while the molybdenum can be deposited from the [(Ni)(MoO$_4$)(Na)(Cit)]$^{2-}$ complex only. Hence, the only factor which can affect the molybdenum amount in the alloy is [(Ni)(MoO$_4$)(Na)(Cit)]$^{2-}$ concentration in the plating bath. This multicomplex compound occurs based on the reaction given in the literature [19, 36–38] by the following reaction;

$$(NiCit)^- + [(MoO_4)(Cit)(Na)]^{4-}$$
$$\rightarrow [(Ni)(MoO_4)(Na)(Cit)]^{2-} + (Cit)^{3-} \quad (IV)$$
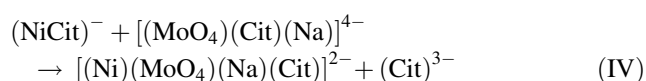
It can be concluded that (NiCit)$^-$ and [(MoO$_4$)(Cit)(Na)]$^{4-}$ species must be formed in the electrolyte for the mentioned reaction to be performed. At this point, citrate plays an important role, and it is important to know which citrate species is predominant in the plating bath. In this type of electrolyte, there are two factors that influence citrate species. The first one is the citrate concentration, and the second one is the pH value to wit NH$_3$ concentration. Since the citrate concentration in the electrolyte was already kept constant for all experiments, the effect of electrolytic pH value stands out. (Cit)$^{3-}$ anions are necessary to create (NiCit)$^-$ and [(MoO$_4$)(Cit)(Na)]$^{4-}$ complexes. Eliaz [36] reported that when NH$_3$ is not added to the electrolyte, the predominant citrate species become (Cit)$^{3-}$ for the pH range of 7–9. Thus, choosing a value of pH = 8 can ensure stable operation [36]. If the pH level is above 10.5, (Cit)$^{4-}$ anions start to be the dominant species [36]. Consequently, the rate of reaction (IV) as well as molybdenum amount in the alloy will decrease. However, NH$_3$ is also a well-known ligand forming complexes with Ni, Co, Fe, and many other metals. When NH$_3$ is added to the plating bath for setting the pH, [Ni(NH$_3$)$_n$]$^{2+}$ complex can be formed, which is another precursor for Ni deposition [37, 38]. This time, Ni^{2+} cations bind to both of the ligands (NH$_3$ and citrate). Hence, the concentration of (NiCit)$^-$ species will decrease. In such a case, the rate of reaction (IV) and molybdenum amount in the alloy decrease again. Lehman [27] has reported that an increase in the pH value of the bath from 8 to 11 leads to an increase of Ni deposition rate and decrease in Mo content in the Ni–Mo alloy. These results are consistent with this study; this means that the optimum amounts of (NiCit)$^-$ and [(MoO$_4$)(Cit)(Na)]$^{4-}$ species in the codeposited process at 9.5 pH for maximum Mo wt% in alloy was obtained.

The polarization curve 6 in Fig. 1 shows Ni–Mo coatings which electrodeposited under the same conditions as for the curve 5 but recorded for total of 60 min of hydrogen evolution at the current density of −100 mA cm^{-2} prior to the polarization test. It can be seen in Table 2 that the HER

overpotential value at -100 mA cm^{-2} (η_{100}) was reduced significantly with hydrogen evolution on the surface, which suggests the activation of electrode due to HER. This can be explained by removal of any existing corrosion products from the pores during hydrogen gas evolution [21, 39]. In terms of the existence of an oxide film on the surface, which inhibits the electron transfer, larger overpotentials are required for HER to occur. When HER on the sample surface was increased before the polarization measurement from 10 to 60 min, Ni–oxide layer was removed during the cathodic treatment, thus oxide-free surface was reached, and in turn, the symmetry factor β value (or transfer coefficient, $\alpha = 1 + \beta$ in this case) was increased.

Finally, the polarization curve 7 shows Ni–Mo coatings that is the electrodeposited nickel on copper plate (Cu/Ni/NiMo–sample 7) under the same condition as sample 6. It can be seen that the HER activity of coating was improved. This indicates that the existence of a thin under-layer of Ni coating provides an extra stability and activity to the cathode material. Similar effects have been reported for NiZn coatings [39] where hydrogen generators were produced.

As mentioned earlier, since Ni curve and Ni–Mo samples of 1, 2, and 3 in Fig. 1 do not show any significant changes in slope, the same HER reaction mechanism should be valid through the entire overpotential region investigated. As seen in b values, samples of 4, 5, 6, and 7 in Table 2, in contrast to others, the polarization curves recorded on this Ni–Mo samples display two potential-dependent regions related to the HER. In low and high hydrogen overpotential ranges, the Tafel slopes varied between -36 and -71 and -143 and -196 mV dec^{-1}, respectively (Table 2). The change of the b value with polarization has also been reported in the literature [20, 22, 29, 32–34, 40]. The fundamental reason for this transition could be related to the depletion of the d-electron density at the Fermi level of the NiMo alloys by adsorbed hydrogen, which remains partially uncompensated at lower overpotentials [32–34]. It has been recently shown that the reaction mechanisms of the HER on Ni- and Ni-based alloys are a consecutive combination of Volmer and Heyrovsky step [41]. However, in lower potential range with low coverage by H$_{ads}$ intermediates, the decrease of Tafel slope indicates that Heyrovsky step controls the rate of the overall reaction. When the cathodic polarization is increased from lower to higher overpotentials, the d-electron density at the Fermi level increases and $\theta_H \rightarrow 1$, thus enhances the kinetics of the Heyrovsky step, and consequently the Volmer step (proton discharge reaction) becomes the rds at high overpotentials. It is also possible for the observed diffusion like shapes of the Tafel curves that NiMo-hydride forms on the surface which acts as a barrier for further hydrogen evolution [34, 42, 43].

As discussed previously, the Tafel curves describe a few comparative data of information regarding the electrocatalytic activity of the investigated cathodes, such as b, α, j_0. The smaller Tafel slope is preferential because minor change in electrode overpotential results in a larger increase in HER current, and thus faster hydrogen gas production. At the same time, the electron transfer coefficient and exchange current density values are desired to be as large as possible. It can be seen in Table 2 that as wt% of Mo content in the alloy is increased, the α and j_0 values increased while b value decreased. According to this data, it can be seen that in sample 7 (Cu/Ni/NiMo), hydrogen evolution reaction was enhanced at surface at both low and high current density area.

In addition, the overpotential (i.e., energy input) at a fixed current density which are directly proportional to the rate of hydrogen evolution or vice versa can be a more practical parameter for characterizing and comparing the apparent electrode activity. It can be seen from Table 2 that the Ni electrode has the highest η_{100} and the lowest j_{100} values compare to NiMo electrodes. In addition, a significant increase of catalytic efficiency is evident for sample 7 that exhibits the lowest values of η_{100}, and the highest values of j_{100}. In conclusion, all the analysis parameters presented in Table 2, which are related to the Tafel curves in Fig. 1, display the same trend and clearly show the evidence that sample 7 electrode is the most active in HER among the investigated materials.

3.2 Surface morphology

The surface morphologies of sample 3, 4, and 5 (Cu/NiMo) and 7 (Cu/Ni/NiMo) are displayed in Fig. 2. Overall image is homogenous. Round-shaped NiMo electrodeposits grew two-dimensionally at a 2/3 Ni/Mo ratio. The NiMo phase is composed of round particles with sizes ranging from ca. 2 μm to 5 μm on the surface (Fig. 2a). Figure 2b, c appears very similar to each other, however the morphology is different than the sample 3 films (Fig. 2a). The SEM pictures of samples 4 and 5 clearly show that the surface of the deposits was relatively smooth. It can be said that both coatings have grown two-dimensionally. On the other hand, the Ni–Mo coating obtained onto the Cu/Ni substrate (Fig. 2d) is a cauliflower-like morphology, and this 3D structure is an indication that Cu/Ni/NiMo has higher surface area available for the HER. This films has some holes at higher magnification (inset Fig. 2d) which may attributed to hydrogen bubbles formed during codeposition and large agglomerations of typical nodular grains.

When polarization characteristics of electrodes in Fig. 1, chemical compositions in Table 1 and SEM images in Fig. 2 are considered together, the highest electrocatalytic
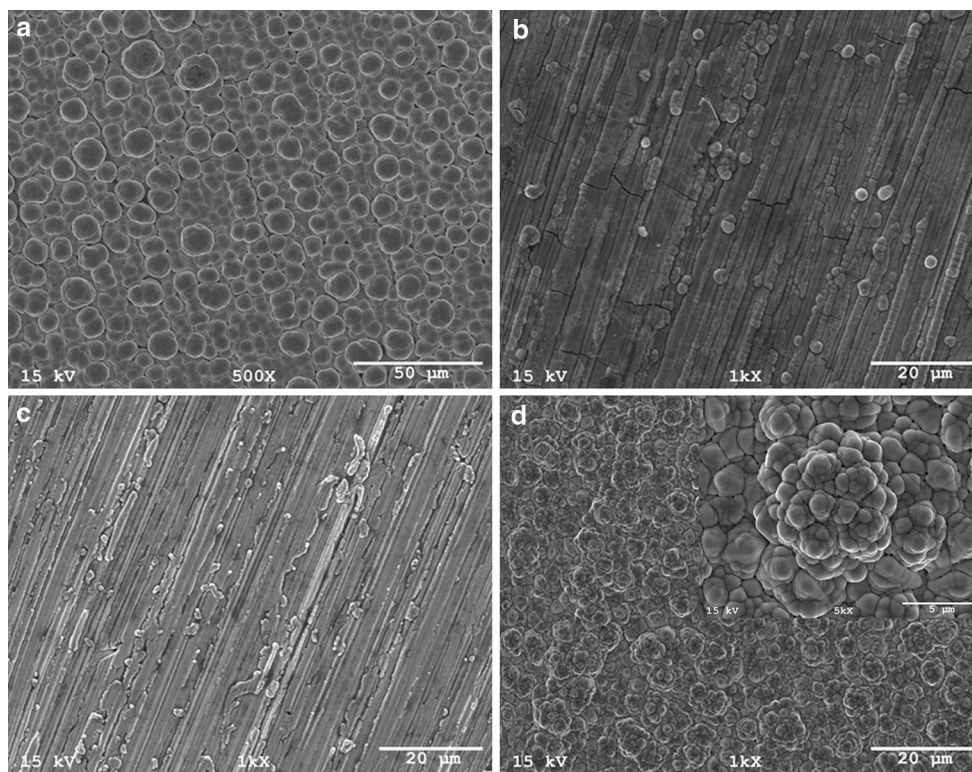
Fig. 2 SEM images of NiMo alloys **a** Cu/3, **b** Cu/4, **c** Cu/5, and **d** Cu/Ni/7

activity was achieved in the electrode where Mo content was the highest, and the surface morphology was the greatest due to the increase in the ratio of real area/geometric area. Chemical composition determines the electrolytic activity when similar surface properties exist (Fig. 2b, c). On the other hand, when chemical composition is the same, electrolytic activity is determined by the surface morphology (Fig. 2c, d). The interesting observation was the dominant effect of chemical composition over

the HER characteristic rather than the surface morphology. This can be clearly seen from the comparison of HER activity of low Mo and high surface area of Fig. 2a and high Mo and low surface area of Fig. 2c.

3.3 The effect of temperature on HER

Figure 3a shows the polarization curves of Cu/Ni/NiMo (sample 7) and Cu/NiMo (sample 6) (inset Fig. 3a)
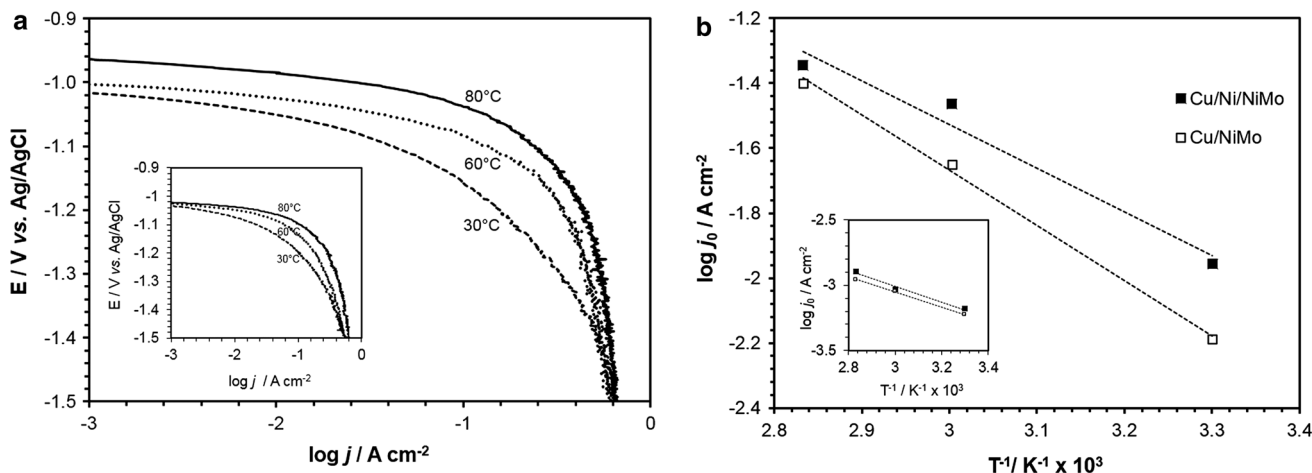

Fig. 3 **a** The polarization curves of Cu/Ni/NiMo and Cu/NiMo (*inset*) electrodes for HER at different temperatures. **b** The Arrhenius plots of the HER on the NiMo electrodes at high and low (*inset*) current density areas

Table 3 HER kinetic parameters obtained by analysis of curves presented in Fig. 3a

T (°C)	$-b_1$ (mV dec^{-1})	$-b_2$ (mV dec^{-1})	η_{100} (mV)	η_{300} (mV)	j_{100} (mA cm^{-2})	j_{300} (mA cm^{-2})
Cu/NiMo						
30	40	143	179	321	34.8	264.8
60	25	184	125	284	73.4	320.8
80	24	188	77	179	145.3	445.3
Cu/Ni/NiMo						
30	36	145	147	278	47.1	344.3
60	23	168	80	172	141.8	448.6
80	24	198	48	152	198.7	452.1

electrodeposits for HER at different temperatures in 1 M of NaOH solution. Table 3 shows the same kinetic parameters that was determined from Fig. 3. The increase of temperature for both electrodes exhibits an obvious promoting effect on HER, leading to a decreases of overpotential at fixed current density and increase of hydrogen production rate at a constant overpotential. The overpotential of Cu/NiMo at −100 mA cm^{-2} current density at 80 °C is −77 mV, while this value is −48 mV for Cu/Ni/NiMo (Table 3). Han [20] reported the overpotential of NiMo at −200 mA cm^{-2} current density in 33 wt% NaOH solution at 80 °C to be −62 mV. The overpotential of the Ni–Mo is comparable to the other binary coatings. The overpotential at −100 mA cm^{-2} and 25 °C was found to be between −266 mV and −341 mV for NiCo in 6 M KOH [44], −248 mV for NiP in 5 M KOH [45], −268 mV for the NiAl in 1 M NaOH [46], −173 mV for the CoZn in 1 M NaOH [47], and −264 mV for the NiFe in 1 M NaOH [48], −96 mV for the NiCoZn–Pt in 1 M NaOH [49].

The exchange current densities are derived by extrapolation of Tafel slopes to zero overpotential, and the Arrhenius plot is present in Fig. 3b. This curve exhibits a linear relationship, and thus electrochemical activation energies for the HER could be calculated according to the following equation [25]:

$$\log j_0 = \log(FK_C) - \Delta G_0 / 2.303\,RT \qquad (2)$$

where R is the gas constant, and ΔG_0 (kJ mol^{-1}) is the apparent activation energy. The apparent activation energy calculated in low (inset Fig. 3b) and high current density areas for Cu/Ni/NiMo are 11.42 and 25.73 kJ mol^{-1}, respectively, while for Cu/NiMo, the corresponding values are 11.12 and 32.54 kJ mol^{-1}. Han [20] reported that for amorphous Ni–Mo, the activation energies depending on the current density area were 14.05 and 24.99 kJ mol^{-1}.

3.4 EIS analysis of Ni–Mo coatings

The HER on Cu/NiMo (sample 6) and Cu/Ni/NiMo (sample 7) was also investigated by EIS. The EIS measurements were made from 100 kHz to 0.1 Hz at different potentials (−1.20, −1.25, and −1.30 V) for HER. Covering current density range for applied overpotentials to electrodes were ca. from 50 to 300 mA cm^{-2}. As can be seen from Figs. 4 and 5, the correlation between experimental and simulated data is very good enough to apply EIS modeling in all overpotentials.

Figure 4 gives Bode (Fig. 4a) and Nyquist (Fig. 4b) diagrams obtained from Cu/NiMo, and Fig. 5 gives Bode (Fig. 5a) and Nyquist (Fig. 5b) diagrams obtained from Cu/Ni/NiMo. The double layer can be represented by the electrical equivalent circuit diagrams to model the metal/solution interface. A two constant-phase elements (CPE's) serial model (2TS) was used to model the solid/liquid interfaces, and the experimental data were fitted accordingly. The electrical equivalent circuit diagrams are given in inset of Fig. 5b, and the resulting fitting parameters are given in Table 4. The 2TS model has been used to describe a response of the HER on porous electrodes [45, 49]. This model consists of the solution resistance, R_s, in series with two CPE–R elements. According to this model, the high-frequency time constant independent of the potential, described by the R_p and CPE$_p$ connected in parallel, is related to the electrode porosity. The potential-dependent time constant occurring at the low-frequency area is related to HER kinetics and described by R_{ct} and CPE$_{dl}$ [34]. A constant-phase element (CPE) is commonly used to represent capacitances taking into account the roughness and inhomogeneity of the electrode surface. In addition, CPEs, which allow considering the effects of deviations from ideality, were used to fit more accurately the impedance behavior of the electrical double layer and coating. A CPE impedance is described by $Z_{CPE(\omega)} = 1/T\,(j\omega)^n$ where T is the capacitance parameter (the magnitude of the CPE), j is the imaginary unit, ω is the angular frequency, and n is a coefficient associated to the system homogeneity. The capacitance parameter T_{dl} is related to the average double-layer capacitance C_{dl} by the relation [50]:
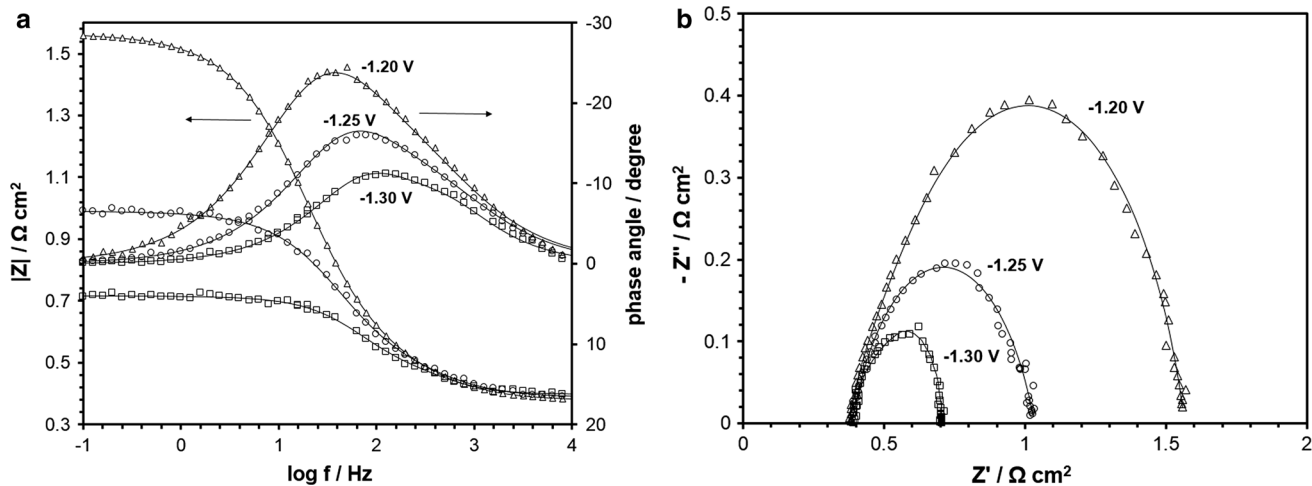
Fig. 4 a Bode and **b** Nyquist diagrams recorded in 1 M NaOH at 25 °C at different potentials for the HER on Cu/NiMo. *Symbols* are experimental data, and *solid lines* are modeled data
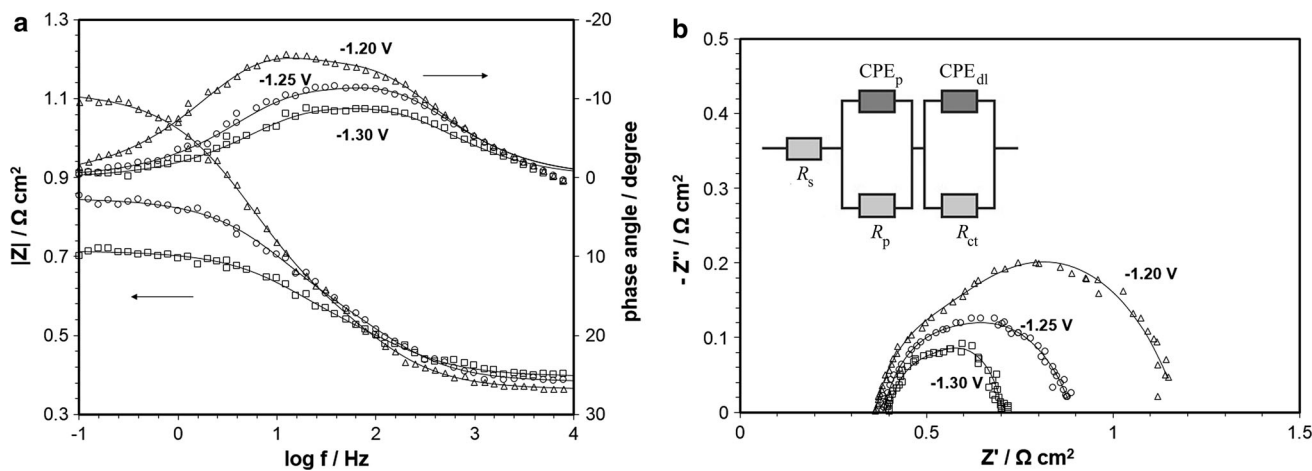

Fig. 5 a Bode and **b** Nyquist diagrams recorded in 1 M NaOH at 25 °C at different potentials for the HER on Cu/Ni/NiMo. *Symbols* are experimental data, and *solid lines* are modeled data. 2TS model used to explain the EIS response of the HER on NiMo electrodes is presented in the *inset* of the Nyquist diagram. R_s solution resistance, R_p resistance of pores, CPE$_p$ constant-phase element corresponding to the capacitance of pores, R_{ct} charge transfer resistance, and CPE$_{dl}$: constant-phase element corresponding to the double-layer capacitance

Table 4 Electrochemical parameters obtained by fitting EIS results at different potentials for NiMo alloys

$-E$(V)	R_s(Ω)	CPE$_p$			CPE$_{dl}$			C_{dl}(μF cm^{-2})	$R_{f(av)}$
		T_p(Ω^{-1} cm^{-2} s^n)	R_p(Ω)	n	T_{dl}(Ω^{-1} cm^{-2} s^n)	R_{ct}(Ω)	n		
Cu/NiMo									
1.20	0.376	0.0296	0.112	0.76	0.027	1.08	0.78	6977	389
1.25	0.387	0.0205	0.089	0.79	0.025	0.51	0.80	7342	
1.30	0.396	0.0071	0.062	0.95	0.023	0.26	0.86	9060	
Cu/Ni/NiMo									
1.20	0.362	0.0438	0.193	0.76	0.158	0.56	0.72	47870	2542
1.25	0.382	0.0353	0.183	0.76	0.162	0.28	0.75	50733	
1.30	0.397	0.0456	0.128	0.75	0.179	0.19	0.75	53942	

$$C_{dl} = \left[T_{dl} / \left(\left(R_s + R_p \right)^{-1} + R_{ct}^{-1} \right)^{(1-n)} \right]^{1/n} \qquad (3)$$

In both of the Bode diagrams (Figs. 4a; 5a), at the mid-frequency region of the frequency phase-angle curves, capacitive loops are observed which are affected by the potential change. These capacitive loops occur due to the condensation behavior of the coating which is created as a result of phase difference between alternative current and potential that takes places at the interface of electrode/electrolyte at the electrochemical double layer. The phase differences changed with different potentials, and this shows that there exists a charge transfer reaction. At the high-frequency region, the capacitive effect (variation in the phase angle) is independent of potential. In this case, the reaction that causes capacitive effect can only be attributed to the surface properties of the electrode.

For a Nyquist diagram, the R_p is corresponding to the high-frequency and the R_{ct} to the low-frequency loops. As seen from Figs. 4b and 5b, and Table 4, the diameter of the high-frequency loop nearly remained the same; however, the diameter of the low-frequency loop strictly depends on the overpotential and reduced with the increasing applied potential. On the other side, the diameter of the low-frequency semicircle on Nyquist plots of Cu/Ni/NiMo is relatively smaller in comparison with the diameter of semicircle obtained for Cu/NiMo at the same overpotential. Such behavior indicates that the value of the charge transfer resistance R_{ct} for Cu/Ni/NiMo is smaller than Cu/NiMo.

From Table 4, it is clear to show the R_{ct} decreased with the overpotential increasing, indicating the potential dependence of R_{ct} for both NiMo films. The low charge transfer resistance at high overpotential is in accordance with the observed high exchange current density for HER.

The electrochemical double-layer capacitance (C_{dl}) of Cu/Ni/NiMo coatings has higher values at the mid-frequency region than Cu/NiMo. C_{dl} value depends on electrode potential, electrolyte temperature, ion concentration, and electrode surface properties. Since these variables are constant, it can be seen that the effect of surface properties stands out as the major factor for the change in the capacitance. In addition, C_{dl} values of both coatings are not affected by the potential variation, nevertheless there is a small deviation with the increased potential. The stabilization of C_{dl} values at different potentials leads to the fact that electrode surface area remained constant at all applied potential levels (Table 4).

The roughness factor for 1 cm^2 geometric area is expressed as $R_f = C_{dl}/20\ \mu F$ [34, 41]. It is important to note that being an ideal value, the average double-layer capacitance of a smooth metal surface is 20 μF cm^{-2} [43, 45]. Clearly, in order to design a good electrocatalysts, one

of the major goals is to achieve a large true surface area per geometric area ratio, i.e., the roughness factor. As it can be seen from Table 4, Cu/Ni/NiMo coating has the highest roughness factor than Cu/NiMo. The surface roughness values were found to be 2542 for Cu/Ni/NiMo and 389 for Cu/NiMo. Similar results were reported in the literature for Cu/Ni/NiMo as 2100 for Ni–Mo alloys on to Ni mesh [21]; between 2052 and 3379 for Ni–Mo [34], 1500 for porous Ni–P + TiO$_2$ [45], 2473 for NiCu [51], while for Cu/NiMo, these were 355 for Ni–Mo on to PANI layer [33], 520 for Ni17Mo7O [52], 423 for Ni–Mo–PE$_{Ni}$ [53].

Since the production of hydrogen in a real hydrogen generator is related to the overall current, one can conclude that Cu/Ni/NiMo really represents the best investigated catalytic coating. Therefore, the electrochemical stability has been tested for industrial applications, and the results are given below.

3.5 Electrochemical stability of Cu/Ni/NiMo electrode

In addition to the electrocatalytic activity, the choice of electrode must also have high corrosion resistance. During shut-down electrolysis, the electrode materials can be corroded and, as a result, may lose their activity as well as life time. Therefore, in order to investigate the corrosion behavior of electrode, CV, current–potential curves, and EIS methods were used. First; the CV of the Cu/Ni/NiMo electrode recorded with the sweep rate of 10 mV s^{-1} in the 1 M NaOH at 25 °C is shown in Fig. 6. The diagram was plotted between oxygen and hydrogen-evolution potentials in order to investigate passive surface layers formed during the anodic and cathodic polarizations and the oxygen evolution potential. It is clear from Fig. 6 that two well-defined anodic peaks (a_1 and a_2) and two cathodic peaks
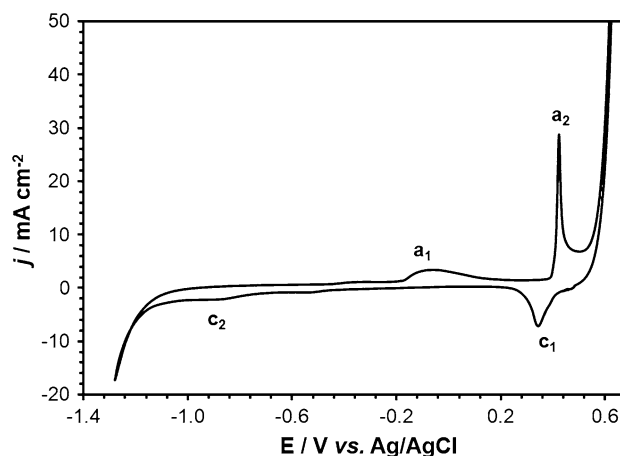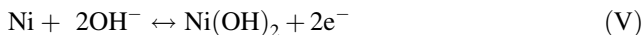

Fig. 6 Cyclic Voltammetry recorded at the sweep rate of 10 mV s^{-1} in 1 M NaOH at 25 °C for Cu/Ni/NiMo electrode

(c_1 and c_2) were obtained in the forward and reverse scans, respectively. On the anodic sweep, the peak a_1 is assigned to the formation of $\alpha - Ni(OH)_2$ according to the following overall reaction [48]:

$$Ni + 2OH^- \leftrightarrow Ni(OH)_2 + 2e^- \qquad (V)$$

The peak (a_2) at +0.4 V corresponds to the Ni^{2+}/Ni^{3+} transitions as given in the following equation [44]:

$$Ni(OH)_2 \leftrightarrow NiOOH + H^+ + e^- \qquad (VI)$$
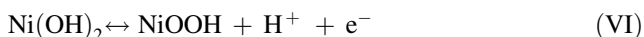
The peaks c_1 and c_2 in the cathodic sweep show the reduction of Ni^{3+} to Ni^{2+} and of the $\alpha - Ni(OH)_2$ back to the metallic Ni, respectively.

On the anodic regions, around +0.6 V and above, the oxygen evolution reaction occurs. It can be concluded that oxygen evolution experiments on the Ni–Mo alloy electrodes must be performed over the +0.6 V to get clear oxygen evolution.

Comparing the CV results of pure Ni [21, 48] and the Ni–Mo electrodes (Fig. 6), it can be said that both electrodes have similar reactions as reactions (V) and (VI) which occurred in the investigated media. No further oxidation of molybdenum oxides or their anodic dissolution to MoO_4^{2-} species were observed.

Figure 7 show the influence of different anodic and cathodic treatments on the Cu/Ni/NiMo alloy HER activity. Curve 1 represents the original Tafel curve which was not exposed to any anodic or cathodic treatment. Right after recording ten cycles of CV (−1.5/+ 0.6 V), the polarization characteristics for the HER on electrode changes are given in curve 2. In addition to CV treatment, same electrode was also exposed to oxygen evolution at 100 mA cm^{-2} for 15 min, and the polarization curve was recorded immediately after oxygen evolution. However, the electrocatalytic properties of the coating was not changed (curve 3). This finding shows that after CV, the
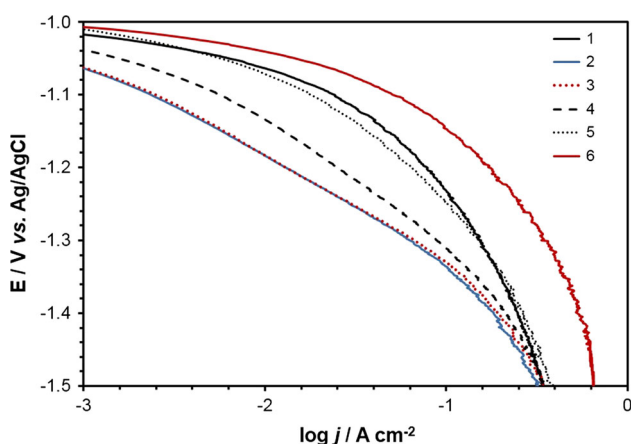
surface was covered with oxide layer, and then additional oxygen evolution on the surface had no effect on the HER activity. After that, the electrode was exposed to HER at −100 mA cm^{-2} (the same current density as that for the oxygen evolution) for 15, 30, and additional 45 min successively, and the polarization curves (curve 4, 5, 6) were recorded immediately after each step. All cathodic treatments enhanced the HER activity of NiMo electrode and polarization curve 5 becomes almost the same as curve 1. However, after anodic treatment, total 90 min of hydrogen evolution at −100 mA cm^{-2}, the electrode completely regained its catalytic activity and showed much better HER activity (curve 6). It is clear from these results presented in Fig. 7 that the oxide layer formed during the anodic treatment could completely be reduced during the hydrogen evolution.

Finally, the corrosion behavior of a Cu/Ni/NiMo electrode to which current was not applied was also investigated. For comparison, EIS curves of Ni electrode was also added. EIS test was applied after the open-circuit potential was reached. The Nyquist plots obtained in 1 M NaOH solution at open-circuit conditions (ca. after 1 h) are given in Fig. 8 while Bode plots as inset in Fig. 8. The shape of Nyquist plots (Fig. 8) of the pure Cu/Ni and Cu/Ni/NiMo coatings were similar with respect to their shape, they only differ considerably in their sizes. This implied that the corrosion process might follow the same mechanism. Since the radius of the semicircle is associated with the resistance of charge transfer reaction at the solution/coating interface, therefore, it can be said that the Cu/Ni/NiMo film exhibits higher corrosion resistance than Cu/Ni coating. The corrosion resistance of nickel was reported in the literature to be improved by the rapid formation of continuous $Ni(OH)_2$ [48] and NiO [39] protective films at surface crystalline
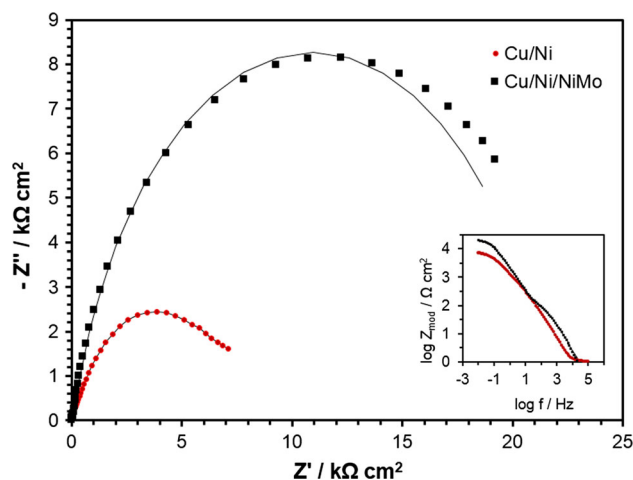

Fig. 7 The polarization curves for the Cu/Ni/NiMo recorded in 1 M NaOH at 30 °C after different anodic and cathodic treatments

Fig. 8 Nyquist plots of Cu/Ni/NiMo at open-circuit potentials, and log Z_{mod} − log f curve of Cu/Ni/NiMo presented as *inset* Nyquist plots

defects and within the pores during immersion. Similar phenomena are probably developing at the Cu/Ni/NiMo electrode surface. However, the open-circuit potential of the Cu/Ni and Cu/Ni/NiMo electrode were −315 and −145 mV after 1 h of exposure, respectively. Hence, the open-circuit potential is nobler for NiMo than Ni film. Thus, when a thin nickel film was coated under a NiMo alloy coating (Cu/Ni/NiMo), the corrosion resistance was considerably enhanced. The charge-transfer resistance (R_{ct}) is a measure of electron transfer across the surface and is inversely proportional to corrosion rate [54]. R_{ct} for Cu/Ni, Cu/Ni/NiMo electrodes were determined as 8.5 and 21.7 kΩ, respectively, using to electrochemical equivalent circuit model (two-time constant parallel model) as described in literature [54]. In addition, the corrosion rate can be estimated by the value of the impedance modulus (Z_{mod}) in the Bode plots. The higher value of Z_{mod} implies a lower corrosion rate of the coatings (inset Fig. 8).

In brief, Cu/Ni/NiMo electrode have a good corrosion resistance in 1 M NaOH at open-circuit potential due to the formation of a passive oxide layer over the electrode surface (Fig. 8). However, the formation of the oxide layer could completely be reduced during the electrolysis through hydrogen evolution (Fig. 7).

4 Conclusions

In this study, Ni and Ni–Mo alloy coatings with various chemical compositions were electrochemically deposited on a copper and on an electrodeposited nickel plate onto copper electrode and characterized by different techniques in view of their possible applications as electrocatalytic materials for the HER in alkaline medium. The electrodeposited Cu/Ni/NiMo alloy coatings exhibit porous surface morphology and much better activity toward the HER than pure Ni electrode. The results showed that the corresponding HER overpotential of the Ni–Mo film depends on alloy composition and surface morphology. NiMo coating with approximately 41 wt% molybdenum content was produced from a bath with a pH of 9.5, Ni/Mo ratio of 1/12, and 0.5 M sodium citrate concentration on electrodeposited Ni onto copper plate. According to the characterization test results, this alloy yielded the highest electrocatalytic activity in the HER, mainly attributed to the higher Mo content and increased surface area. The apparent activation energy for this electrode for high current density areas was calculated to be 25.73 kJ mol^{-1}. It is also shown that during the anodic polarization in 1 M NaOH, the oxidation of the electrode surface occurs that changes the polarization characteristics (increasing overpotential for the hydrogen evolution) of this alloy. When, after such a

treatment, the electrodes were exposed to the hydrogen evolution for a certain time, and almost identical polarization diagrams for the HER were obtained to the ones before any anodic treatment due to the complete removal of the oxide layer. Moreover, this electrode has a good corrosion resistance in 1 M NaOH at open-circuit potential which was preferable for these types of electrodes.

References

1. Veziroğlu TN, Barbir F (1992) Hydrogen: the wonder fuel. Int J Hydrogen Energy 17:391–404. doi:10.1016/0360-3199(92)90183-W
2. Veziroğlu TN, Sxahin S (2008) 21st Century's energy hydrogen energy system. Energy Convers Manag 49(7):1820–1831. doi:10.1016/j.enconman.2007.08.015
3. Döner A, Taşkesen E, Kardaş G (2014) Hydrogen evolution stability of platinum modified graphite electrode. Int J Hydrogen Energy 39:11355–11359. doi:10.1016/j.ijhydene.2014.05.159
4. Solmaz R, Kardaş G (2011) Fabrication and characterization of NiCoZn–M (M: Ag, Pd and Pt) electrocatalysts as cathode materials for electrochemical hydrogen production. Int J Hydrogen Energy 36:12079–12087. doi:10.1016/j.ijhydene.2011.06.101
5. Pletcher D, Li X (2011) Prospects for alkaline zero gap water electrolysers for hydrogen production. Int J Hydrogen Energy 36:15098–15104. doi:10.1016/j.ijhydene.2011.08.080
6. McArthur MA, Jorge L, Coulombe S, Omanovic S (2014) Synthesis and characterization of 3D Ni nanoparticle/carbon nanotube cathodes for hydrogen evolution in alkaline electrolyte. J Power Sour 266:365–373. doi:10.1016/j.jpowsour.2014.05.036
7. Rami A, Lasia A (1992) Kinetics of hydrogen evolution on Ni–Al alloy electrodes. J Appl Electrochem 22:376–382. doi:10.1007/BF01092692
8. Suffredini HB, Cerne JL, Crnkovic FC, Machado SAS, Avaca LA (2000) Recent developments in electrode materials for water electrolysis. Int J Hydrogen Energy 25:415–423. doi:10.1016/S0360-3199(99)00049-X
9. Tang X, Xiao L, Yang C, Lu J, Zhuang L (2014) Noble fabrication of Ni–Mo cathode for alkaline water electrolysis and alkaline polymer electrolyte water electrolysis. Int J Hydrogen Energy 39:3055–3060. doi:10.1016/j.ijhydene.2013.12.053
10. Raj IA, Vasu K (1990) Transition metal-based hydrogen electrodes in alkaline solution-electrocatalysis on nickel based binary alloy coatings. J Appl Electrochem 20:32–38. doi:10.1007/BF01012468
11. Pletcher D, Li X, Wang S (2012) A comparison of cathodes for zero gap alkaline water electrolysers for hydrogen production. Int J Hydrogen Energy 37:7429–7435. doi:10.1016/j.ijhydene.2012.02.013
12. Hu C-C, Weng C-Y (2000) Hydrogen evolving activity on nickel–molybdenum deposits using experimental strategies. J Appl Electrochem 30:499–506. doi:10.1023/A:1003964728030
13. Donten M, Cesiulis H, Stojek Z (2005) Electrodeposition of amorphous/nanocrystalline and polycrystalline Ni–Mo alloys from pyrophosphate baths. Electrochim Acta 50:1405–1412. doi:10.1016/j.electacta.2004.08.028

14. Chassaing E, Portail N, Levy AF, Wang G (2004) Characterisation of electrodeposited nanocrystalline Ni–Mo alloys. J Appl Electrochem 34:1085–1091. doi:10.1007/s10800-004-2460-z

15. Sanches LS, Domingues SH, Marino CEB, Mascaro LH (2004) Characterisation of electrochemically deposited Ni–Mo alloy coatings. Electrochem Commun 6:543–548. doi:10.1016/j.elecom.2004.04.002

16. Crousier J, Eyraud M, Crousier JP, Roman JM (1992) Influence of substrate on the electrodeposition of nickel-molybdenum alloys. J Appl Electrochem 22:749–755. doi:10.1007/BF01027505

17. Sanches LS, Marino CB, Mascaro LH (2007) Investigation of the codeposition of Fe and Mo from sulphate-citrate acid solutions. J Alloy Compd 439:342–345. doi:10.1016/j.jallcom.2006.08.231

18. Marlot A, Kern P, Landolt D (2002) Pulse plating of Ni–Mo alloys from Ni–rich electrolytes. Electrochim Acta 48:29–36. doi:10.1016/S0013-4686(02)00544-3

19. Jović BM, Jović VD, Maksimović VM, Pavlović MG (2008) Characterization of electrodeposited powders of the system Ni–Mo–O. Electrochim Acta 53:4796–4804. doi:10.1016/j.electacta.2008.02.004

20. Han Q, Cui S, Pu N, Chen J, Liu K, Wei X (2010) A study on pulse plating amorphous Ni–Mo alloy coating used as HER cathode in alkaline medium. Int J Hydrogen Energy 35:5194–5201. doi:10.1016/j.ijhydene.2010.03.093

21. Krstajic NV, Jovic VD, Lj Gajic-Krstaji, Jovic BM, Antozzi AL, Martelli GN (2008) Electrodeposition of Ni–Mo alloy coatings and their characterization as cathodes for hydrogen evolution in sodium hydroxide solution. Int J Hydrogen Energy 33:3676–3687. doi:10.1016/j.ijhydene.2008.04.039

22. Aaboub O (2011) Hydrogen evolution activity of Ni–Mo coating electrodeposited under magnetic field control. Int J Hydrogen Energy 36:4702–4709. doi:10.1016/j.ijhydene.2011.01.035

23. Krstajić NV, Lj Gajić-Krstajić, Lačnjevac U, Jović BM, Mora S, Jović VD (2011) Non-noble metal composite cathodes for hydrogen evolution. Part I: the Ni–MoO$_x$ coatings electrodeposited from Watt's type bath containing MoO$_3$ powder particles. Int J Hydrogen Energy 36:6441–6449. doi:10.1016/j.ijhydene.2011.02.105

24. Krstajić NV, Lačnjevac U, Jović BM, Mora S, Jović VD (2011) Non-noble metal composite cathodes for hydrogen evolution. Part II: the Ni–MoO$_2$ coatings electrodeposited from nickel chloride-ammonium chloride bath containing MoO$_2$ powder particles. Int J Hydrogen Energy 36:6450–6461. doi:10.1016/j.ijhydene.2011.02.106

25. Xia M, Lei T, Lv N, Li N (2014) Synthesis and electrocatalytic hydrogen evolution performance of Ni–Mo–Cu alloy coating electrode. Int J Hydrogen Energy 39:4797–4802. doi:10.1016/j.ijhydene.2014.01.091

26. Gennero de Chialvo MR, Chialvo AC (1998) Hydrogen evolution reaction on smooth Ni$(1-x)$ + Mo(x) alloys $(0 \leq x \leq 0.25)$. J Electroanal Chem 448:87–93. doi:10.1016/S0022-0728(98)00011-4

27. Beltowska-Lehman E, Indyka P (2012) Kinetics of Ni–Mo electrodeposition from Ni-rich citrate baths. Thin Solid Films 520:2046–2051. doi:10.1016/j.tsf.2011.10.024

28. Jaksic JM, Vojnovic MV, Krstajic NV (2000) Kinetic analysis of hydrogen evolution at Ni–Mo alloy electrodes. Electrochim Acta 45:4151–4158. doi:10.1016/S0013-4686(00)00549-1

29. Kaninski MPM, Miulovic SM, Tasic GS, Maksic AD, Nikolic VM (2011) A study on the Co–W activated Ni electrodes for the hydrogen production from alkaline water electrolysis—energy saving. Int J Hydrogen Energy 36:5227–5235. doi:10.1016/j.ijhydene.2011.02.046

30. Herraiz-Cardona I, Ortega E, García Antón J, Pérez-Herranz V (2011) Assessment of the roughness factor effect and the intrinsic catalytic activity for hydrogen evolution reaction onNi-based electrodeposits. Int J Hydrogen Energy 36:9428–9438. doi:10.1016/j.ijhydene.2011.05.047

31. Los P, Rami A, Lasia A (1993) Hydrogen evolution reaction on Ni-Al electrodes. J Appl Electrochem 23:135–140

32. Highfield JG, Claude E, Oguro K (1999) Electrocatalytic synergism in Ni–Mo cathodes for hydrogen evolution in acid medium: a new model. Electrochim Acta 44:2805–2814. doi:10.1016/S0013-4686(98)00403-4

33. Damian A, Omanovic S (2006) Ni and Ni–Mo hydrogen evolution electrocatalysts electrodeposited in a polyaniline matrix. J Power Sources 158:464–476. doi:10.1016/j.jpowsour.2005.09.007

34. Navvaro-Flores E, Chong Z, Omanovic S (2005) Characterization of Ni, NiMo, NiW and NiFe electroactive coatings as electrocatalysts for hydrogen evolution in an acidic medium. J Mol Catal A 226:179–197. doi:10.1016/j.molcata.2004.10.029

35. Jaksic MM (2000) Hypo–hyper–d–electronic interactive nature of synergism in catalysis and electrocatalysis for hydrogen reactions. Electrochim Acta 45:4085–4099. doi:10.1016/S0360-3199(00)00120-8

36. Eliaz N, Gileadi E (2007) The mechanism of induced codeposition of Ni–W alloys. Electrochem Society 6:337–349

37. Metzler OY, Zhu L, Gileadi E (2003) The anomalous codeposition of tungsten in the presence of nickel. Electrochim Acta 48:2551–2562. doi:10.1016/S0013-4686(03)00297-4

38. Eliaz N, Sridhara TM, Gileadi E (2005) Synthesis and characterization of nickel tungsten alloys by electrodeposition. Electrochim Acta 50:2893–2904. doi:10.1016/j.electacta.2004.11.038

39. Solmaz R, Kardaş G (2007) Hydrogen evolution and corrosion performance of NiZn coatings. Energy Convers Manag 48:583–591. doi:10.1016/j.enconman.2006.06.004

40. Conway BE, Jerkiewicz G (2000) Relation of energies and coverages of underpotential and overpotential deposited H at Pt and other metals to the volcano curve for cathodic H$_2$ evolution kinetics. Electrochim Acta 45:4075–4083. doi:10.1016/S0013-4686(00)00523-5

41. Krstajić N, Popović M, Grgur B, Vojnović M, Šepa D (2001) On the kinetics of the hydrogen evolution reaction on nickel in alkaline solution Part I. The mechanism. J Electroanal Chem 512:16–26. doi:10.1016/S0022-0728(01)00590-3

42. Hu W (2000) Electrocatalytic properties of new electrocatalysts for hydrogen evolution in alkaline water electrolysis. Int J Hydrogen Energy 25:111–118. doi:10.1016/S0360-3199(99)00024-5

43. Metikos-Hukovic M, Jukic A (2000) Correlation of electronic structure and catalytic activity of Zr–Ni amorphous alloys for the hydrogen evolution reaction. Electrochim Acta 45:4159–4170. doi:10.1016/S0013-4686(00)00550-8

44. Elumalai P, Vasan HN, Munichandraiah N, Shivashankar SA (2002) Kinetics of hydrogen evolution on submicron size Co, Ni, Pd and Co–Ni alloy powder electrodes by d.c. polarization and a.c. impedance studies. J Appl Electrochem 32:1005–1010. doi:10.1023/A:1020935218149

45. Łosiewicz B, Budniok A, Rówiński E, Łagiewka E, Lasia A (2004) The structure, morphology and electrochemical impedance study of the hydrogen evolution reaction on the modifed nickel electrodes. Int J Hydrogen Energy 29:145–157. doi:10.1016/S0360-3199(03)00096-X

46. Hitz C, Lasia A (2001) Experimental study and modeling of impedance of the her on porous Ni electrodes. J Electroanal Chem 500:213–222. doi:10.1016/S0022-0728(00)00317-X

47. Döner A, Solmaz R, Kardaş G (2011) Enhancement of hydrogen evolution at cobalt–zinc deposited graphite electrode in alkaline solution. Int J Hydrogen Energy 36:7391–7397. doi:10.1016/j.ijhydene.2011.03.083

48. Solmaz R, Kardaş G (2009) Electrochemical deposition and characterization of NiFe coatings aselectrocatalytic materials for alkaline water electrolysis. Electrochim Acta 54:3726–3734. doi:10.1016/j.electacta.2009.01.064

49. Birry L, Lasia A (2004) Studies of the hydrogen evolution reaction on Raney nickel–molybdenum electrodes. J Appl Electrochem 34:735–749

50. Kubisztal J, Budniok A, Lasia A (2007) Study of the hydrogen evolution reaction on nickel-based composite coatings containing molybdenum powder. Int J Hydrogen Energy 32:1211–1218. doi:10.1016/j.ijhydene.2006.11.020

51. Solmaz R, Döner A, Kardaş G (2008) Electrochemical deposition and characterization of NiCu coatings as cathode materials for hydrogen evolution reaction. Electrochem Commun 10:1909–1911. doi:10.1016/j.elecom.2008.10.011

52. Kawashima A, Sakaki T, Habazaki H, Hashimoto K (1999) Ni–Mo–O alloy cathodes for hydrogen evolution in hot concentrated NaOH solution. Mater Sci Eng, A 267:246–253. doi:10.1016/S0921-5093(99)00099-4

53. Niedbala J, Budniok A, Lagiewka E (2008) Hydrogen evolution on the polyethylene-modified Ni–Mo composite layers. Thin Sol Films 516:6191–6196. doi:10.1016/j.tsf.2007.11.105

54. Özkan S, Hapçı G, Orhan G, Kazmanlı K (2013) Electrodeposited Ni/SiC nanocomposite coatings and evaluation of wear and corrosion properties. Surf Coat Technol 232:734–741. doi:10.1016/j.surfcoat.2013.06.089